Supplemental Material

Adhesive wear mechanisms in the presence of weak interfaces: Insights from an amorphous model system

Tobias Brink *and* Jean-François Molinari

Civil Engineering Institute and Institute of Materials Science and Engineering,
École polytechnique fédérale de Lausanne (EPFL), Station 18, CH-1015 Lausanne, Switzerland

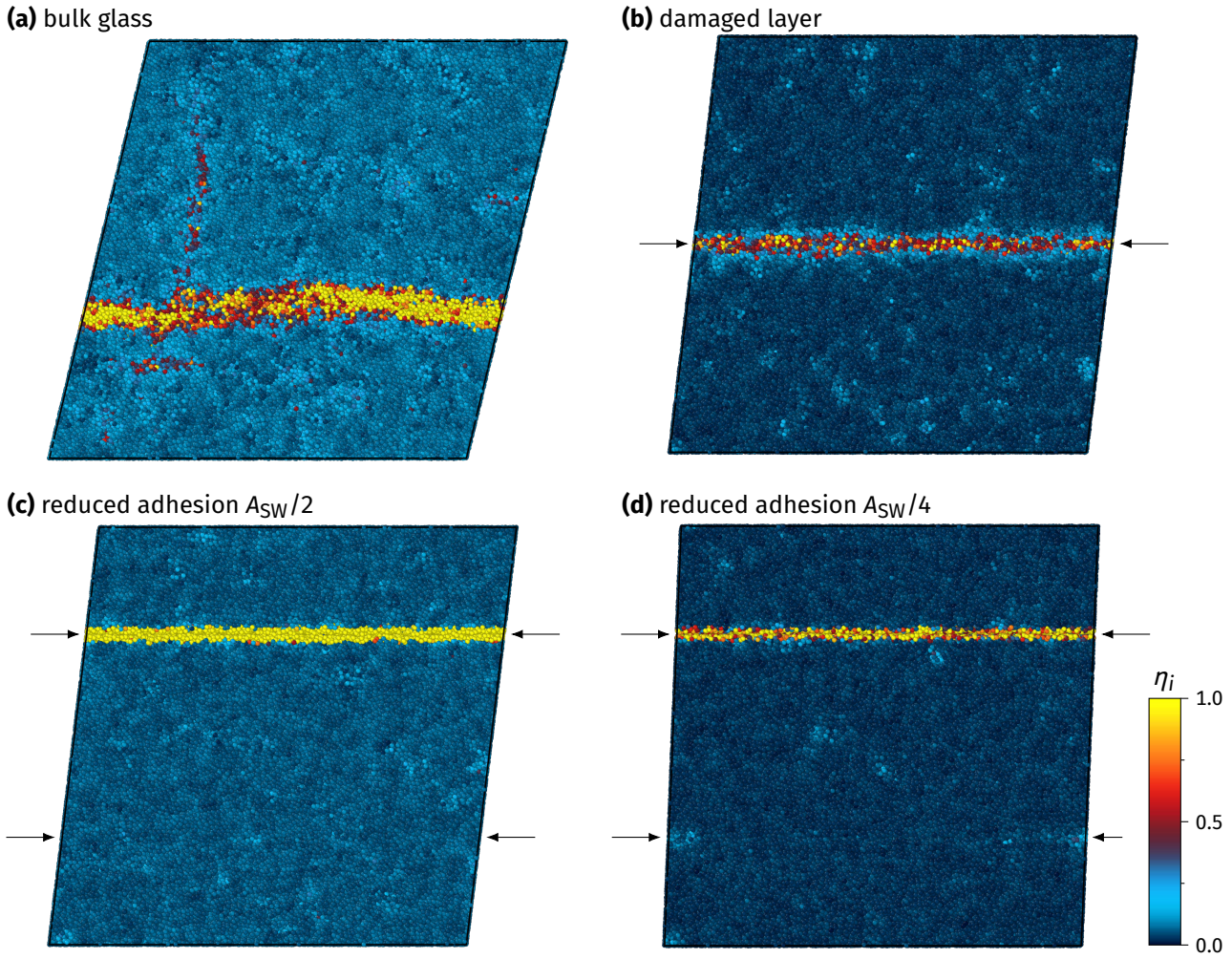

Fig. S.1: Snapshots of bulk shear tests with periodic boundary conditions. All simulation boxes have a size of roughly $20 \times 20 \times 20\,\mathrm{nm}^3$. (a) Homogeneous bulk glass at a macroscopic shear strain of $\gamma = 24\%$, color coded according to the local atomic shear strain η_i. A single, dominant shear band is visible. (b) Simulation with a damaged layer (arrows) of width 1 nm at $\gamma = 12\%$. The shear band is forced onto the plane of the damaged layer, but some diffuse plasticity can be observed around the shear band. (c)–(d) The simulations with interfaces were modeled by two identical material blocks with a reduced adhesion potential between them. Due to the periodic boundary conditions, this results in two interface planes (arrows). Slip is completely confined to one of these two planes and no significant plasticity is observed next to the interface. The snapshots were taken at shear strains of 12% (c) and 4% (d), respectively.

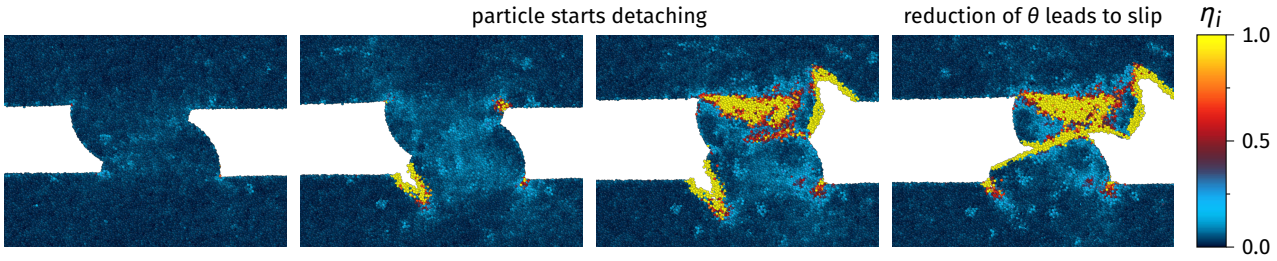

Fig. S.2: Slip after partial wear particle detachment due to decreasing inclination. Snapshots from a simulation with interface adhesion strength of $\tilde{\tau}_{\mathrm{adh}} = 0.7\,\tilde{\tau}_b$, $d = 10\,\mathrm{nm}$, $p_N = 0.1\,\tilde{\tau}_b$, and initial $\theta = 30°$. At the onset of fracture, $\theta = 25°$. As soon as the interface rotates to $\theta \approx 15°$, slip sets in.

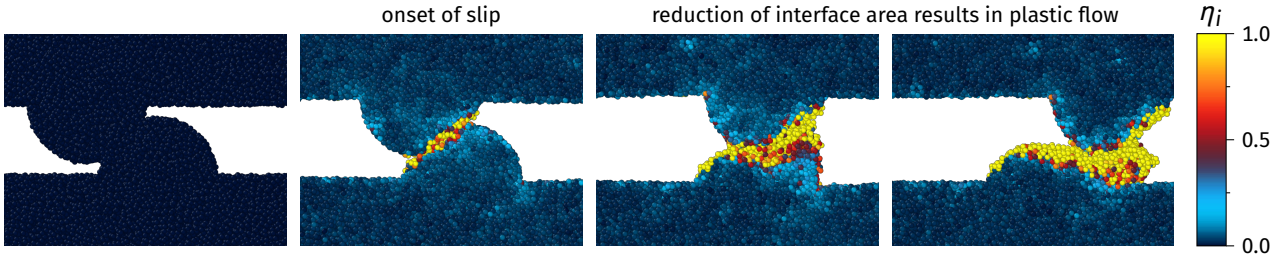

Fig. S.3: Plastification during slip due to increasing normal pressure. Snapshots from a simulation with interface adhesion strength of $\tilde{\tau}_{\mathrm{adh}} = 0.15\,\tilde{\tau}_b$, $d = 5\,\mathrm{nm}$, $p_N = 0.1\,\tilde{\tau}_b$, and initial $\theta = 45°$. The junction area reduces after the onset of slip, leading to an increase of p_N and plastic flow.

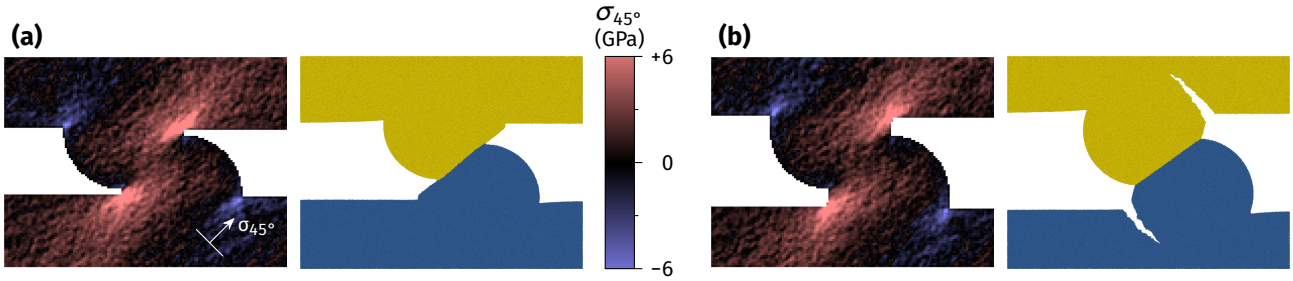

Fig. S.4: Sensitivity of the interface to stress concentrations. Simulations with interface adhesion strength of $\tilde{\tau}_{\mathrm{adh}} = 0.15\,\tilde{\tau}_b$, $d = 30\,\mathrm{nm}$, $p_N = 0.1\,\tilde{\tau}_b$, and initial $\theta = 45°$. (a) If the inclination θ is high, its edge can come close to the stress concentration at the corner of the asperity. This seems to lead to the nucleation of a slip front even in cases where our model predicts particle detachment. (b) By putting the asperities on small "sockets" (height $\approx d/10$), the stress concentrator is moved away from the junction interface and a wear particle detaches, as expected. The latter procedure was performed for the simulations with initial $\theta \geq 45°$ in Fig. 5(c) and (d).

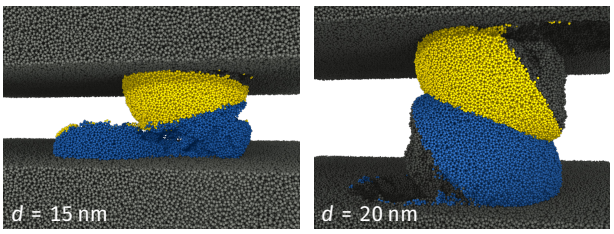

Fig. S.5: Snapshots of simulations where the interface is stronger than the bulk of the asperities. Simulations were prepared by randomly removing 5% of atoms in the asperities, keeping the 2-nm-wide interface intact. This reduces the bulk shear strength to 6.9 GPa and the shear modulus to roughly 45 GPa, resulting in $d^* \approx 17\,\mathrm{nm}$. The simulations displayed on the left (initial $\theta = 30°$) confirm this value.

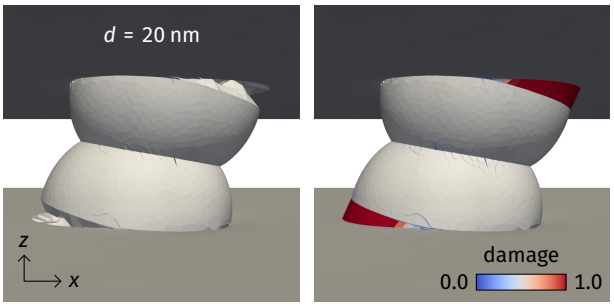

Fig. S.6: FEM simulation of a contact junction without weakened interface. The left image shows only the solid, while the right image includes the cohesive elements. The cracks appear, as expected, at the bottom of the asperities and lead to the detachment of a wear particle.

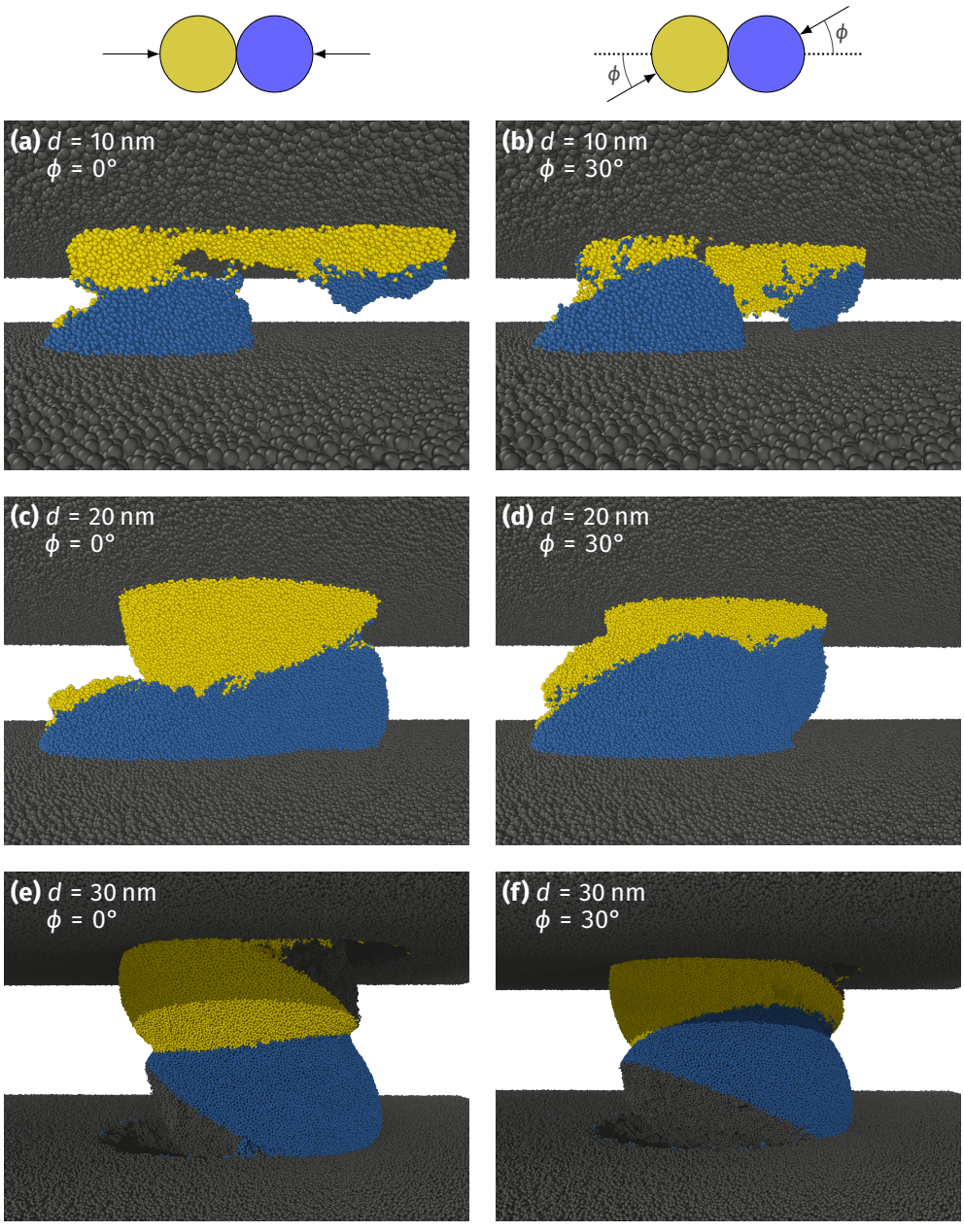

Fig. S.7: Simulations with a sliding direction deviating from the xz plane. It can be seen here—as expected from the derivation in Appendix B—that the mechanism is unchanged for a rotation of the sliding direction by $\phi = 30°$: Asperities with $d \leq 20\,\text{nm}$ plastify (a)–(d), while asperities with $d = 30\,\text{nm}$ form wear particles (e)–(f), independent of ϕ.